An experimental investigation of free and submerged miniature liquid jet array impingement heat transfer

A.J. Robinson [a, c, *], E. Schnitzler [b]

a Department of Mechanical and Manufacturing Engineering, Parsons Building, Trinity College Dublin, D2, Ireland
b IUP Génie des Systémes Thermiques, Université de Pau et des Pays de l'Adour, Pau 64000, France
c CTVR, Lloyd Institue, Trinity College, Dublin 2, Ireland

Abstract

Liquid water jet impingement cooling was investigated experimentally for both free-surface jet arrays and confined submerged jet arrays. The jet arrays consisted of straight holes of 1.0 mm diameter arranged in rectangular arrays with spacings of 3, 5 and 7 jet diameters between adjacent jets. For the impingement surface area of 780 mm^2, these jet array configurations can be considered well populated, with a total of 21, 45 and 121 jets impinging on the surface. Average heat transfer and pressure drop measurements are presented for volumetric flow rates in the range of 2 L/min $\leq \dot{V} \leq$ 9 L/min and dimensionless jet-to-target spacings between $2 \leq H/d_n \leq 30$. For the submerged jet arrays a strong dependence on both jet-to-target and jet-to-jet spacing is observed and correlations are presented that adequately predict the experimental measurements. The free-surface jets show a non-monotonic change with jet-to-target spacing with a local minimum in the heat transfer coefficient at approximately H/d_n = 10. Here a transition from a submerged to a free jet flow configuration occurs.

Once again, a correlating equation is presented that adequately predicts the free-surface jet array heat transfer data. The pumping power required to form the submerged and free jet flows show a different relationship to the heat transfer coefficient. Generally, submerged jets have a higher heat transfer coefficient for a given pumping power requirement.

Keywords: Jet impingement cooling; Liquid jet arrays; Electronics cooling

Nomenclature

A_r surface area coverage ratio defined in Table 1

C constants in Eq. (4)

d_n jet diameter (m)

d_i impingement diameter (m)

f friction factor

g gravitational acceleration (m/s^2)

H distance between orifice plate and impingement surface (m)

$\bar{h}$ surface averaged heat transfer coefficient (W/m^2 K)

k thermal conductivity (W/m K)

L^* characteristic length defined in Table 1 (m)

L_e length of a unit cell in Eq. (4)

L heater length in Eqs. (2) and (4) (m)

L_c characteristic length (m)

m exponent on Reynolds number (Eq. (4)), exponent on S/d_n (Eq. (14))

n exponent on Reynolds number (Eq. (4)), exponent on H/d_n (Eq. (14))

N number of jets on orifice plate (–)

Nu Nusselt number (–)

ΔP pressure drop across orifice (Pa)

Pr Prandtl number (–)

$Q_{pumping}$ pumping power (W)

Re Reynolds number (–)

S jet–to–jet spacing (m)

t thickness of nozzle plate (m)

T temperature (°C or K)

V_n nozzle exit velocity (m/s)

V_i impingement velocity (m/s)

$\dot{V}$ volumetric flow rate (m^3/s)

k_f fluid thermal conductivity (W/m K)

q^n heat flux (W/m^2)

z location of thermocouple (m)

Subscripts

f fluid

film   film temperature

jet   jet

s surface

t top thermocouple in block

Greeks

μ dynamic viscosity (kg m/s)

ρ density (kg/m^3)

ν kinematic viscosity (m^2/s)

1. Introduction

All electronic devices dissipate heat during their normal operation and this self-heating can adversely affect device performance and reliability. Thermal management is a particular constraint in computer processors, radio transmitters, optical devices and numerous other technologies. The current trend towards faster switching speeds and greater on chip functionality is leading to greater chip heat generation with significant non-uniformities in on-chip heat flux. If the heat generated by an electronic component is not spread and subsequently dissipated to the surroundings efficiently, the component will heat up to unacceptable temperature levels causing damage and/or failure of the component. To put this into perspective, for silicon devices and other electronic components such as electrolytic capacitors, the life expectancy roughly doubles for every 10 °C reduction in temperature. The ramifications with regards to reliability of the electronic component are obvious. It is now well established that thermal issues are presenting one of the most serious roadblocks to component miniaturisation and processor speed.

From a thermal standpoint, adding direct liquid cooling in the form of impinging liquid jets has many attractive features for electronics thermal management. This is largely due to the fact that impinging jets have one of the highest known single-phase heat transfer coefficients. As such, liquid jet impingement cooling offers the desirable property of very high heat flux removal rates with small surface-to-coolant temperature differentials. Furthermore, the pressure drop across the nozzle that is required to form the jets is not necessarily related to the heat transfer mechanisms occurring at the impingement surface [1]. This is in contrast to liquid cooling strategies such as two-phase microchannel flow where the heat transfer, void fraction and pressure drop are all interrelated. This desirable characteristic presents the possibility of optimising the jet configuration for minimal volumetric flow rate and pumping power [1]. Another noted advantage of direct liquid jet impingement cooling is the possible elimination of a layer of thermal interface material between the electronic component and the next level of the thermal package. This is crucial for some high-power applications where the contact resistance can be the most severe blockage to heat flow of the entire thermal solution.

A significant body of literature exists for single circular impinging jet heat transfer and flow dynamics for both air and liquids [2–9]. Generally, the heat transfer coefficient on the impingement surface has a bell-shaped distribution with the local maximum occurring at the stagnation point. The heat transfer coefficient decreases symmetrically with radial distance from the stagnation point. Researchers have found that secondary peaks or enhancement in the heat transfer coefficient are often present for both gas and liquid impingement cooling [6]. The secondary peaks are typically found in the region of 1.5–2.5 jet diameters from the stagnation point. The secondary peaks have been accounted for in many studies as being due to a transition to turbulence in the wall jet region [7]. It has been determined that the magnitude and distribution of the heat transfer coefficient depends on several parameters including but not limited to the Reynolds number (Re), Prandtl number (Pr), jet-to-target spacing (H/d_n), jet diameter (d_n), degree of confinement, as well as the physical geometry of the jets and target surface. Compared with single impinging jets, the heat transfer and flow characteristics of jet arrays have received much less attention over the past two decades. This is especially true for liquid jet array impingement.

For the cases studied here, jet array impingement heat transfer can be grouped into two categories: free-surface jet impingement and confined-submerged jet impingement. The two flow configurations are illustrated in Fig. 1 for jet arrays. For each case the liquid is discharged across a nozzle plate that is perforated with orifices. For the free surface jet impingement configuration (Fig. 1a) the liquid jets discharge into an ambient gas and impinge normally on the surface. Submerged jets issue into a region containing the same liquid at rest (Fig. 1b). Compared to free surface jets, the heat transfer to submerged jets is much more sensitive to the jet-to-target spacing. Submerged jets are also influenced by the presence of a confining plate. The jets are confined if the radial spread is restricted in a narrow channel bounded by the impingement surface and the nozzle plate (Fig. 1b). The heat transfer coefficient on the impingement surface for jet arrays has a more complex distribution than for single jets since the interaction of neighbouring jets can influence the heat transfer.
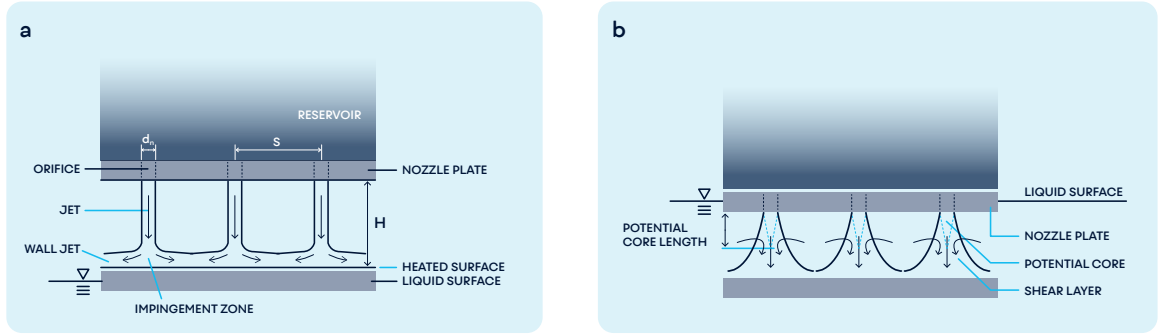
Fig 1. Free-surface (a) and confined-submerged (b) jet array configurations

In particular, the heat transfer is dependent on the jet-to-jet spacing, S/d_n. In an array configuration each jet forms a cell or module that has within it a jet flow region comprised of the stagnation and near-stagnation radial flow zones. Here, the heat transfer coefficient distribution is similar to that discussed above for single jets. However, each module is surrounded by a region of radial flow interaction that influences the heat transfer positively due to enhanced mixing and associated turbulence. Here, local maxima in the heat transfer coefficient distribution have been observed [13] resulting in an undulating heat transfer coefficient profile along the heated surface.

Analytic predictions of the heat transfer to free surface jets have been carried out by Yonehara and Ito [10] for square arrays of water jets impinging on an isothermal surface. It was assumed that each impinging jet formed an individual cell or module. The local and average heat trans- fer rates were determined for repeating modules surrounding each jet in the array. The average heat transfer to an individual impinging jet, as characterized by the module- average Nusselt number, was given as,

$$Nu_{d_n} = 2.38 Re_{d_n}^{2/3} Pr^{1/3} (S/d_n)^{-4/3}$$

(1)

Agreement with experimental measurements was adequate and diverged somewhat for jet-to-jet spacings above $S/d_n \geq 13.8$ and $Re_{dn} \leq 48\ 000$, although following the $(S/d_n)^{-4/3}$ dependence.

Kiper [11] was one of the earliest investigators to promote impinging liquid jet arrays as a viable cooling technology for electronic devices. Expanding on the work of Martin [3] for air jet arrays, Kiper [11] demonstrated that scaling the impinging fluid jet array heat transfer technology to small flow passage dimensions, and using water as the coolant, the convective heat transfer coefficients was significantly higher than conventional liquid cooling technologies such as immersion cooling. It was noted that the fundamental limit of this technology is the pressure drop penalty across the nozzle plate.

Heater surface-average heat transfer correlations for arrays of four and nine free surface jets impinging on square 12.7 mm × 12.7 mm heat sources has been provided by Jiji and Dagan [12]. The nozzles were drilled and reamed straight channels of 0.5 mm and 1.0 mm diameters. Using FC-77 and water as the coolants, they found that the heat transfer rate was independent of the jet-to-target spacing in the range 3 mm $\leq z \leq$ 10 mm. They correlated the average Nusselt number as

$$Nu_L = 3.84 \left[0.008 \frac{L}{d_n} N + 1 \right] Re_{d_n}^{1/2} Pr^{1/3}$$

(2)

Since the jets were well drained, there was negligible cross-flow between neighbouring jets and each jet established a cell that behaved thermally as a single isolated impinging jet. This is characterised by a high stagnation heat transfer coefficient that decreases sharply in the radial direction along the surface. For a given flow rate per heat source, decreasing the jet diameter resulted in improved

heat transfer as a result of the increase in the stagnation heat transfer coefficient. Adding more jets resulted in a decrease in the jet velocity per heat source by a reduction in the stagnation heat transfer coefficient. However, this could be more than offset by an improvement in the temperature uniformity of the heat source by decreasing the distance between stagnation points. Although not measured, it was pointed out that practical consideration should be given to the fact that a decrease in the jet diameter can drastically increase the pumping power requirement. This is due to the fact that, for a fixed volumetric flow rate, decreasing the jet diameter results in an increase in the jet velocity and subsequent pressure drop across the orifice. Conversely, for a fixed volumetric flow rate and jet diameter, increasing the number of jets per heat source can result in some moderate pumping power reduction since the jet velocity and subsequent pressure drop is reduced.

The effect of jet spacing was more closely examined by Pan and Webb [13]. The local heat transfer distribution for a 9 jet in-line array and a 7 jet staggered array were investigated for dimensionless jet-to-jet spacings of S/d_n = 2, 4, 6, and 8 with water as the coolant. They concluded that, for the central jet module, the stagnation point heat transfer coefficient was independent of jet-to-jet spacing but was found to exhibit a dependence on jet-to-target spacing. Increasing the jet-to-target spacing from 2 to 5 ostensibly changed the flow condition from a confined-sub- merged jet flow to a free-surface jet flow. Pan and Webb determined a Reynolds number dependence very similar to that of Yonehara and Ito [10]. For the central jet module area (not the heater area) the average Nusselt number was correlated as,

$$Nu_{d_n} = 0.225 \ Re_{d_n}^{2/3} \ Pr^{1/3} e^{-0.095(S/d_n)}$$

<div align="right">(3)</div>

Consistent with the observations of [13], the heat transfer was determined to deteriorate with increasing jet-to-jet spacing.

Womac et al. [14] considered both free-surface and confined-submerged jet impingement heat transfer using water and FC-77 as the coolant liquids. Both 2 × 2 and 3 × 3 arrays of circular jets were tested for jet diameters of 0.513 mm and 1.02 mm and several jet-to-jet spacings. The results for the free-surface jets indicated that heat transfer was unaffected by jet-to-target spacing in the range $5 \leq H/d_n \leq 10$. For a fixed volumetric flow rate, the heat transfer improved for decreasing dn and N due to an increase in the jet velocity. For a fixed volumetric flowrate, d_n and N, the heat transfer improved with decreasing jet-to-jet spacing. This finding was attributed to enhancement due to neighbouring cells interfering with one another and/or a possible reduction in the area coverage of the wall jet region of each cell. The later would increase the average heat transfer coefficient of each cell tending towards the stagnation heat transfer coefficient.

For confined-submerged liquid jet arrays, the heat transfer coefficient was found to be relatively insensitive to jet- to-target spacing within the range $2 \leq H/d_n \leq 4$. Generally, the heat transfer to the submerged jets was found to degrade for small ($H/d_n \leq 2$) and large ($H/d_n \geq 10$) separations, depending on jet-to-jet spacing. For ostensibly the same conditions, the submerged jets performed equally as well or better than the free jets. The heat transfer model developed by Womac et al. assumed that each impinging jet formed an individual cell that contained two distinct heat transfer regions. In the centre of a cell is the impingement zone where the heat transfer is governed by the stagnation characteristics of the jet which is impinging normally to the surface. The rest of the cell is comprised of the forced convective region where the heat transfer is governed by the wall jet which flows parallel to the surface.

Womac et al. correlated their data with an area-weighted combination of expressions for the impingement and wall jet regions over the entire heated surface:

$$\frac{Nu_L}{Pr^{0.4}} = C_1 Re_{d_n}^m \left(\frac{L}{d_n}\right) A_r + C_2 Re_{L^*}^n \left(\frac{L}{L^*}\right)(1-A_r) \tag{4}$$

where L is the heater length, L^* is an estimate of the average distance associated with radial flow in the wall jet regions and A_r is the ratio of the effective area of the impingement regions on the heater to the total area of the surface. Table 1 outlines the parameters in Eq. (4), where L_e is the length of a unit cell. Womac et al. cautioned that for small enough jet-to-jet spacing it is possible that the total calculated area coverage of the impingement zone can exceed the total area of the heated surface. In this case A_r is greater than unity and Eq. (4) in its current form gives invalid result, especially considering that the wall jet portion of Eq. (4) will be negative, which is infeasible. For cases where $A_r > 1$ Womac et al. suggest assigning a value of $A_r = 1$. Physically, this implies that within each module a wall jet region does not exist and the heat transfer is only occurring within the impingement zone which is of a dimension that is less than that specified in Table 1. It should also be noted that for the submerged case, Eq. (4) is only valid for small jet-to-target spacings within the range of $2 \leq H/d_n \leq 4$.

Table 1: Parameters for Eq. (4)

	Free Jets	Submerged Jets
C_1	0.516	0.509
C_2	0.344	0.0363
m	0.5	0.5
n	0.579	0.8
L^*	$L^*=\frac{1}{4}(\sqrt{2}+1)L_e-\frac{1}{2}d_i$	$L^*=\frac{1}{4}(\sqrt{2}+1)L_e-(1.9d_n)$
A_r	$A_r=N\pi d_i^2/4L^2$	$A_r=N\pi(1.9d_n)^2/L^2$
	$d_i=\left(V_n d_n^2/V_i\right)^{0.5}$	
	$V_i=\left(V_n^2+2gH\right)^{0.5}$	

Although alluded to in previous works [11,12], Fabbri and Dhir [1] are perhaps the first investigators to measure both pressure drop and heat transfer to impinging liquid jet arrays. With regards to electronics cooling, the practical implication is that a properly designed jet array nozzle will provide the cooling requirement with a minimum volumetric flow and/or pumping power. For free jets, the optimal configuration depends on the geometry and thermal constraints of the device being cooled and the nozzle geometric and flow parameters, such as jet diameter, jet-to-jet spacing and Reynolds number. Fabbri and Dhir investigated microjet arrays ($69~\mu m \leq d_n \leq 250~\mu m$) using water and FC40 as the coolants. They determined that the average surface heat transfer coefficient improved with increasing Re_{d_n} and Pr and decreasing dimensionless jet-to-jet spacing, S/d_n. They also found that the heat transfer to the microjet arrays was significantly larger than for miniature and mesoscale jets ($d_n > 500~\mu m$) for the same volumetric flow rate. In similar form to Pan and Webb [13], they correlated the heat transfer data as,

$$Nu_{d_n} = 0.043~Re_{d_n}^{0.78}~Pr^{0.48} e^{-0.069(S/d_n)} \tag{5}$$

which shows a stronger dependence on the Reynolds number than in previous investigations. It was noted, however that previous studies used larger jets ($d_n > 500~\mu m$) with nozzle arrays that were significantly less populated with jets.

Based on pressure drop measurements, Fabbri and Dhir [1] correlated the friction factor as,

$$f = 0.507 + \frac{189.9}{Re_{d_n}} \tag{6}$$

Given a particular electronics cooling requirement, such as the maximum power that must be removed the dimensions of the device and the maximum allowable junction temperature, Eqs. (5) and (6) can be implemented to determine the jet array design that renders the optimal performance with regards to minimum pumping power or volumetric flow rate.

At present, there are limited measurements of the heat transfer and pressure drop characteristics of free-surface and confined-submerged liquid jet arrays. With regards to electronic packaging where the space claim of the thermal package will likely be restricted, the pumping power and the degree of confinement of submerged and free jet arrays are areas that certainly need to be explored in greater detail. Furthermore, most of the available correlations are developed for small heater surfaces with very few jets impinging on them and are presented without information about the pressure drop.

This work focuses on the heat transfer and pressure drop associated with a large number of liquid miniature jets impinging on a heated surface. Different jet-to-jet and jet-to-target spacings for both confined-submerged and free-surface flow configurations are investigated. Correlations are presented which adequately predict the heat transfer and pressure drop measurements over the range of parameters investigated in this study.

2. Experimental apparatus and instrumentation

The surface average heat transfer coefficient and pressure drop associated with confined–submerged and free–surface water jets have been measured for dimensionless jet–to–target spacings of $2 \leq H/d_n \leq 30$, dimensionless jet–to–jet spacings of $3 \leq S/d_n \leq 7$ and Reynolds numbers within the range of $650 \leq Re_{dn} \leq 500$. The experimental apparatus depicted in Fig. 2 consists of a water delivery and monitoring systems and a test chamber which contains the jet array nozzle and a heated impingement surface.

2.1 Flow delivery and monitoring system

The water flow loop depicted in Fig. 2 consisted of a pump which drew deionized water from a 20 L water reservoir. A constant water temperature was ensured by immersing a coiled heat exchanger into the reservoir. The water flow rate was controlled by a bypass valve prior to being routed to a rotameter (0–10 LPM ± 1.5% FS). The temperature of the water at the inlet of the test chamber was measured with a 1.5 mm diameter sheathed T–type thermocouple in conjunction with a Fluke54II Thermometer (±0.3 °C). The jet exit temperature was assumed to be equal to the temperature that had been measured upstream of the nozzle plate.

As depicted in Fig. 3, the water entered the test chamber through a 170 mm length of 19 mm inner diameter straight tubing that was expanded to a 70 mm long × 80 mm inner diameter plenum prior to being ejected through the jet nozzle plate. The jet nozzles were 3.0 mm thick plastic that were sketched in a commercial 3-D CAD package and subsequently printed using an InVisionTM 3-D Printer. The interchangeable nozzle plates were fastened to the plenum holder by eight screws with a crushed O–ring face seal to ensure that the water was forced through the jet array. This arrangement is shown in the embedded photograph in Fig. 3. Straight through holes of 1.0 mm diameter were fabricated within a circular diameter equal to that of the heated surface (D = 31.5 mm) and special care was taken to ensure that the jets impinged normally on the heated sur face. Nozzle plates with jet–to–jet spacings of 3.0 mm, 5.0 mm and 7.0 mm were fabricated for this study. For the three jet–to–jet spacings tested, the number of jets were N = 21, 45 and 121 respectively.
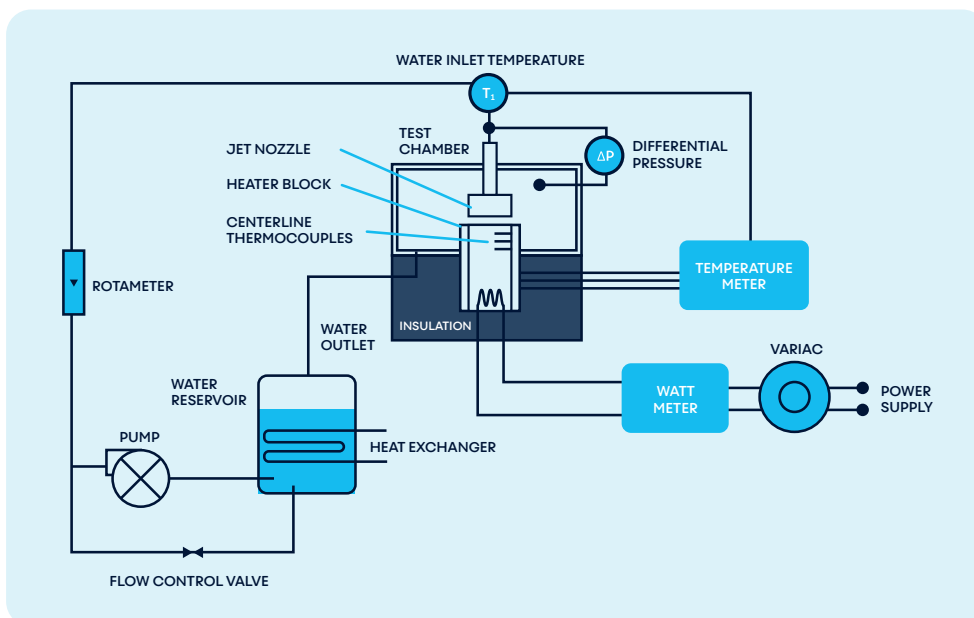

Fig 2. Schematic of jet impingement heat transfer apparatus

2.2 Test chamber

The test chamber facilitated both the measurement of the pressure drop across the jet nozzle and the average heat transfer coefficient from a heated block to the impinging water jets. A Digitron 2083P (0–2 bar ± {0.1% rdg + 0.1%FS}) differential pressure meter was installed between pressure taps located on either side of the jet nozzle in order to measure the associated pressure drop (Figs.2 and 3). Average heat transfer coefficients were determined by directing the jets perpendicular to the instrumented heater block depicted in Fig. 3.
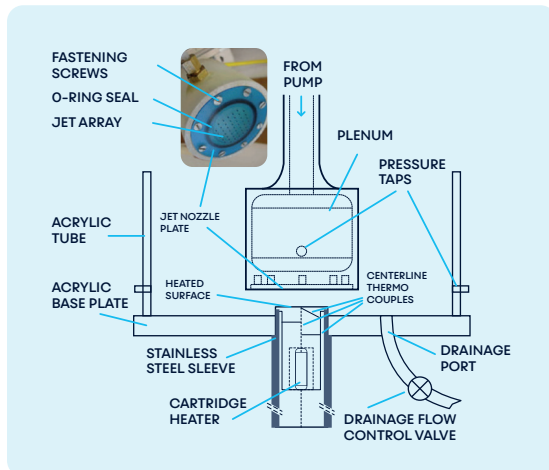

Fig 3. Schematic diagram of test chamber.

A single instrumented heater block was manufactured for this study. The heater block was constructed from a cylindrical bar of ultra pure copper. The upper end of the block was machined flat and served as the heater surface with an exposed diameter of D = 31.5 mm. Below the heater surface the diameter of the block was reduced in order to provide an insulating air gap between the copper block and the stainless steel sleeve and to provide a space for the thermocouple wires to exit. The steel sleeve was then laser welded to the block. The outer periphery of the heater section was subsequently wrapped with sufficient fibreglass insulation to diminish radial heat losses from the block and ensure one-dimensional heat flow to the exposed heated surface. The cylindrical heater block was inserted into a through hole that was machined into a 20 mm thick acrylic sheet. The heater surface protruded approximately 5 mm above the acrylic sheet to allow for drainage through four 15 mm diameter drainage ports. A 193 mm diameter × 300 mm long acrylic tube was fixed to the upper side of the acrylic base plate in order to contain the water and thus force it to exit the vessel through the drainage ports which were gravity fed back to the water reservoir. In order to control the liquid level within the vessel, flow control valves were installed between the drainage ports and the water reservoir. Since the test section container was clear it facilitated visual monitoring of the liquid level within the chamber. For the submerged jet configurations the flow control valves were adjusted so that the liquid level was kept approximately 5 mm above the bottom of the jet nozzle plate. For the free-jet configuration the flow control valves were fully open so that the liquid level remained at or below the level of the heated surface.

The heater block was heated by three 6.35 mm diameter × 44.45 mm long cartridge heaters that were inserted into holes drilled into the bottom of the heater block. The power to the cartridge heaters was adjusted to the desired level by a variable transformer. The current and voltage supply to the heaters were monitored by two Metrix MX22 multimeters (0–400VAC ± 1% rdg, 0–10 A ± 2.5% rdg). The combined maximum power rating of the cartridge heaters was 300 W which was sufficient to provide a high enough heat flux along the block to the surface that accurate determination of the centreline temperature distribution and surface temperature could be measured. This was achieved by inserting three 1.0 mm type-E thermocouples into holes spaced 9.5 mm apart. Each thermocouple well terminated at the block centreline and the top thermocouple was located 1.6 mm from the impingement surface. All thermocouple readings within the block were monitored by a Fluke 54II digital thermometer (±0.3 °C). All measurements were recorded once steady-state conditions were reached.

3. Data Reduction

The average heat transfer coefficient at the heated surface was determined with the expression,

$$\bar{h} = \frac{q''}{\left(T_s - T_{jet}\right)} \quad (7)$$

The heat flux at the surface was assumed to be uniform and was calculated from,

$$q'' = -k_{Cu} \left.\frac{dT}{dz}\right|_{\text{best fit}} \quad (8)$$

where k_{Cu} is the thermal conductivity of the copper which was evaluated at the average block temperature and $dT/dz|_{\text{best fit}}$ is the linear regression fit to the centreline temperature measurements shown in Fig. 3. As detailed in [19], the uncertainty in the heat flux measurement was determined to be ±4.1%. Measurement of the centreline temperature gradient also facilitated the determination of the surface temperature, T_s, also required in Eq. (7) for calculating the heat transfer coefficient. The surface temperature was determined by linear extrapolation of the temperature distribution to the surface,

$$T_s = T_t + (z_s - z_t) \left(\left.\frac{dT}{dz}\right|_{\text{best fit}}\right) \quad (9)$$

where $z_s - z_t$ is the distance from the surface to the location of the top thermocouple. The uncertainly in the surface temperature measurement was estimated to be ±1.2% [19]. The post-calibrated temperature difference ($T_s - T_{jet}$) uncertainty was estimated to be 2%. With the heat transfer coefficient calculated using Eq. (7), the surface-average Nusselt number was determined as,

$$Nu_L = \frac{\bar{h} L_c}{k_f} \quad (10)$$

where the characteristic length for the heater surface was chosen as L_c = D/2 = 15.75 mm. Since only one jet orifice diameter was tested in this study, the Nusselt number based on the jet diameter can be related to Eq. (10) through $Nu_{dn} = (d_n/L_c)Nu_L = 0.0635 Nu_L$. The thermal conductivity of the liquid was evaluated at the film temperature $T_{film} = 0.5 (T_s + T_{jet})$.

The jet Reynolds number was determined from the average jet velocity calculated from the measured water flow rate. The jet velocity and thus the jet Reynolds number can then be calculated using the equations,

$$V_n = \frac{4\dot{V}}{N\pi d_n^2} \qquad (11)$$

and

$$Re_{d_n} = \frac{V_n d_n}{V_{film}} \qquad (12)$$

In this study the pressure drop was recorded for each test. Based on the data, the friction factor was calculated using the expression,

$$f = \frac{\Delta P}{\left(\frac{1}{2}\rho V_n^2\right)\left(\frac{t}{d_n}\right)} \qquad (13)$$

All fluid properties in the above expressions were evaluated at the water film temperature.

The experimental uncertainties of the main parameters are listed in Table 2. The maximum and minimum uncertainties on the Reynolds number and friction factor occur for the case of the lowest and highest flow rates tested respectively. The dimensions t and d_n have an uncertainty of ±10 μm which is the resolution of the 3-D printer.

4. Results and discussion

4.1 Heat transfer

4.1.1 Submerged-confined jet arrays

Fig. 4 shows the surface averaged Nusselt number results versus Reynolds number for the submerged and confined jet configuration for varying jet-to-target spacing and jet-to-jet spacing. Here the drainage flow control valves were adjusted to keep the liquid level within the vessel approximately 5 mm above the plane of the nozzle plate as depicted in Fig. 1b. The correlation proposed by Womac et al. [14], as given by Eq. (4) is also plotted in the figures. Since Womac's correlation is only strictly valid for $2 \le H/d_n \le 4$, the agreement between the correlation and experimental data for $S/d_n = 5$ and 7 at small separation distances of $2 \le H/d_n \le 3$ provides confidence in the efficacy of the experimental procedure and data analysis technique utilised in this investigation. The discrepancy for $S/d_n = 3$ is due to the fact that the effective impingement heat transfer area exceeds the total surface area of the heated surface. As discussed earlier, the area ratio A_r in Table 1 is greater than unity for which [14] suggest assigning a value of $A_r = 1.0$. Albeit an improvised resolution to the problem, general agreement between the measurements and Womac's correlation at $S/d_n = 3$ is observed. However, the discrepancy indicates that the accuracy of Womac's correlation is not assured and should be used with caution when the geometric condition of $A_r > 1$ is reached.

Table 2: Experimental uncertainties

Nu_L	Re_{dn}		f	
	(2 LPM)	(9 LPM)	(2 LPM)	(9 LPM)
7%	10%	5%	20%	12%

Average heat transfer correlations for submerged and confined liquid jet arrays that include variations in the Reynolds number, jet-to-target spacing as well as the jet-to-jet spacing do not currently exist. As a result, an attempt was made here to correlate the experimental data of this investigation. It has been well established in previous investigations [14] that the Prandtl number dependence approximately follows a $Nu_L \propto Pr^{0.4}$ relationship. Choosing this as the appropriate Prandtl number dependence, several different functions were evaluated and the following expression provided an uncomplicated relationship that

$$\frac{Nu_L}{Pr^{0.4}} = 23.39 Re_{d_n}^{0.46} \left(\frac{S}{d_n}\right)^m \left(\frac{H}{d_n}\right)^n \tag{14}$$

As will be discussed, separate values of the exponents m and n are proposed for the regions $2 \le H/d_n \le 3$ and $5 \le H/d_n \le 20$ in view of the distinct trends noted in these regions:

$$\left.\begin{array}{l} m=-0.442 \\ n=-0.00716 \end{array}\right\} \quad 2\le \frac{H}{d_n} \le 3, \ 3\le \frac{S}{d_n} \le 7$$

$$\left.\begin{array}{l} m=-0.121 \\ n=-0.427 \end{array}\right\} \quad 5\le \frac{H}{d_n} \le 20, \ 3\le \frac{S}{d_n} \le 7 \tag{15}$$

Fig. 5 shows a comparison of the prediction of Eq. (14) with the experimentally determined surface averaged Nusselt number of this investigation. As it is shown, the correlations predict nearly all of the experimental data with 92% of the data points falling within the ±15% band.
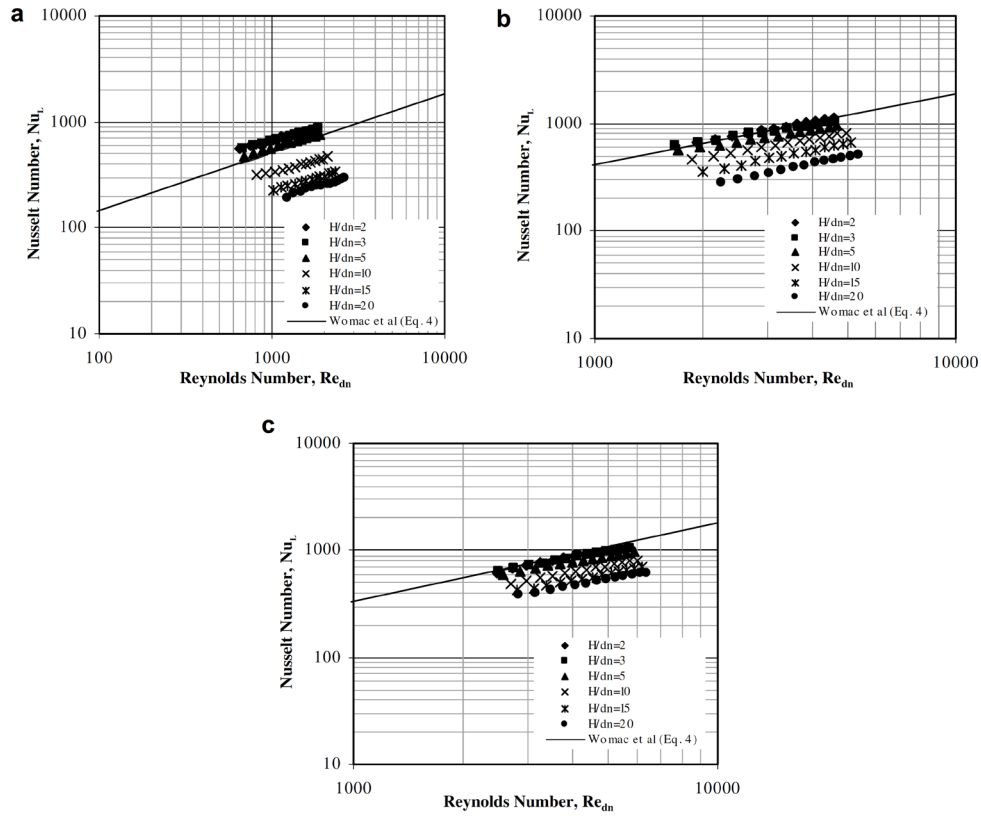
Fig 4. Confined and submerged jet flow. Nusselt number versus Reynolds number for different jet-to-target spacings: (a) S/d_n=3; (b) S/d_n=5; and (c) S/d_n=7

It is evident from Fig. 4 that for $2 \leq H/d_n \leq 3$ the surface averaged heat transfer is relatively insensitive to increasing jet-to-target spacing. This is due to the fact that the heated surface is situated within the length of the potential core of the jets [15]. The length of the potential core (Fig. 1b) is the distance from the orifice exit to the point in the core where the shear layer has penetrated to the centreline of the jet. Within the potential core the centreline velocity is equal to the jet velocity at the exit plane of the orifice. Beyond the potential core length the centreline velocity diminishes while the turbulence increases substantially [15]. The potential core strikes the surface when the jet-to-target spacing is smaller than the core length which is roughly H/d_n = 5 [6]. Since the jet velocity within the potential core is nearly that of the exit velocity from the orifice, the local heat transfer is not expected to vary significantly with initial increases in jet-to-target spacing for small spacings. As expected, Eq. (14) shows a weak dependence on jet-to-target spacings when the heater surface is located within the potential core of the jets, given that $Nu_L (H/d_n)^{-0.00716}$ for $2 \leq H/d_n \leq 3$. This result is consistent with the work of Garimella and Nenaydykh [16] who determined a $Nu_L \propto (H/d_n)^{-0.007}$ relationship, albeit for a semiconfined single jet of FC-77 for the case when $1 \leq H/d_n \leq 5$. Fig. 4a–c show that for each jet-to-jet spacing tested, there is a significant reduction in the Nusselt number for large jet-to-target spacings beyond approximately H/d_n~5. This occurs because the impingement surface is situated beyond the potential core of the jet and the impingement velocity of the fluid in the stagnation region significantly diminishes with increasing jet-to-target spacing due to entrainment of the surrounding liquid [15]. This reduction in the jet velocity adversely affects the local and surface averaged heat transfer in the range $5 \leq H/d_n \leq 20$ as is highlighted by the increase in the magnitude of the exponent to n =-0.427 in Eq. (14). This is somewhat smaller than the $Nu_L \propto (H/d_n)^{-0.566}$ dependence that was predicted for semiconfined single jets by Garimella and Nenaydykh [16] for $5 \leq H/d_n \leq 14$. This is likely due to a slight improvement in the surface average heat transfer of jet arrays over that of single jets due to enhanced turbulence as the result of the mixing of neighbouring jets prior to impingement and/or interactions in the wall jet region. For a fixed Re_{dn} and H/d_n, the measurements indicate that for confined-submerged flow, increasing the jet-to-jet spacing, S/d_n, has a detrimental effect on the heat transfer.
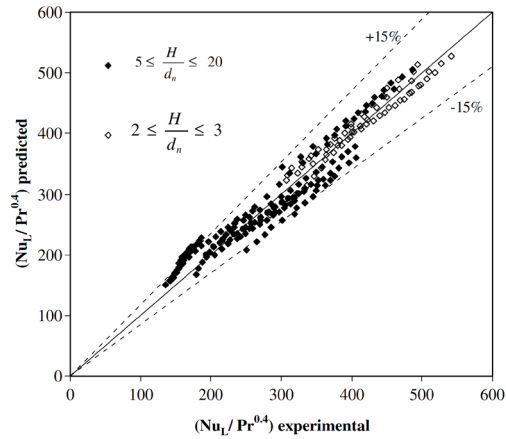
Fig 5. Comparison of the experimental and predicted Nusselt number for confined-submerged jet arrays.

This is evident from the fact that m < O in Eq. (14). This result is consistent with the observations made for free-surface jets [1,13]. As discussed earlier, in an array configuration the heat transfer coefficient distribution is undulating in nature with local maxima occurring at the stagnation points of each jet and a secondary maxima along the periphery of each jet module due to the radial flow interaction of neighbouring jets. It is likely that increasing the spacing between jets would increase the distance between these regions of high heat transfer thus deteriorating the overall heat transfer from the surface with increasing S/d_n. It is interesting to note that the heat transfer dependence on the jet-to-jet spacing, S/d_n, also depends on the jet-to-target spacing.

This is generally not the case for free surface jets where the jet-to-jet spacing dependence is not influenced significantly by the jet-to-target spacing [1]. For small jet-to-target spacing ($2 \leq H/d_n \leq 3$) the heat transfer shows a strong dependence, following $Nu_L \propto (S/d_n)^{-0.442}$. When the surface is located outside of the potential core this dependence reduces to $Nu_L \propto (S/d_n)^{-0.121}$. The reason for this is unclear and will require further investigation. However, it is likely that the observed phenomenon is due to the fact that for small jet-to-target spacings ($2 \leq H/d_n \leq 3$), the high surface average heat transfer coefficient is dominated by the heat transfer to the impinging jet in the impingement region.

Here, a very high local heat transfer coefficient will occur at the stagnation zone that will diminish rapidly with radial distance from the stagnation point. Increasing the jet-to-jet spacing, i.e. decreasing the total number of jets, eliminates the number of stagnation regions available, and since they are the key heat transfer regions, one would expect the dependence on the jet-to-jet spacing, S/d_n, to be quite significant. For larger H/d_n, the diminished velocity and spreading of the jets, combined with the possible interaction of neighbouring jets before striking the surface, result in a local distribution of heat transfer coefficient (and surface temperature) that is significantly more uniform than for the close jet-to-target spacings.

This has been observed by Brevet et al. [17] for confined and submerged jet arrays with air as the coolant. Here, the dominant mechanism of heat transfer is forced convection to a well mixed turbulent jet array that is spatially less variable at the impingement surface. Although one would expect a dependence on the jet-to-jet spacing, one would not expect it to be as severe as with the small jet-to-target spacings, as is consistent with the observations here.

4.1.2 Free-surface jet arrays

Fig. 6 shows the surface averaged Nusselt number results versus Reynolds number for the free-surface jet configuration for varying jet-to-target spacing and jet-to-jet spacing. Here the drainage flow control valves were fully open so that the liquid level within the vessel was at or below the plane of the heated surface. The correlating equations of Pan and Webb [13], Womac et al. [14] and Fabbri and Dhir are also included in the figure. The correlation proposed by Jiji and Dagan [12] in Eq. (2) was deemed not general enough to compare with the present results. Agreement with the correlating equations (Eqs. (3)-(5)) is acceptable. For the higher jet-to-target spacings ($H/d_n \geq 10$) the Nusselt number data are generally lower than predicted by Pan and Webb [13] and Womac et al. [14]. In the present study the volumetric flow rate of the water was considerable and there was a comparatively high population of jets impinging on the surface (N = 21, 45, 121). This is compared to previous studies where there were typically between 4 and 9 jets per heat source [12–14].

Furthermore, in all but [14], the jets were kept well drained since there were far fewer of them and the heater surface was orientated vertically [12] or horizontally above the jet nozzle [13]. For the case considered here, with the heater surface mounted horizontally below the jet array, it is likely that the slightly lower Nu_L results for high $H/d_n \geq 10$ is due to bulk warming of the liquid which remains resident on the surface due to poorer surface drainage. The type of arrangement used here is closer to that used by Fabbri and Dhir [1]. Moderate agreement is observed with Eq. (5) even though this work is outside of the parameter range of [1], given that they tested microjet arrays (65 μm $\leq d_n \leq$ 250 μm).
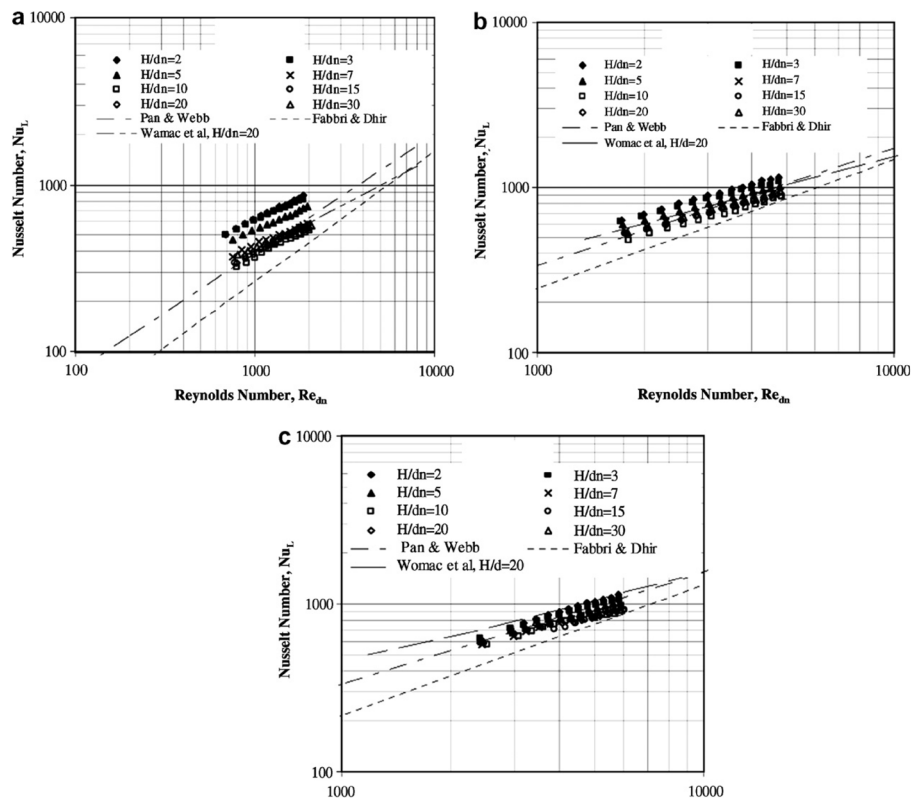

Fig 6. Free-surface jet flow. Nusselt number versus Reynolds number for different jet-to-target spacings: (a) S/d_n=3; (b) S/d_n=5; and (c) S/d_n=7
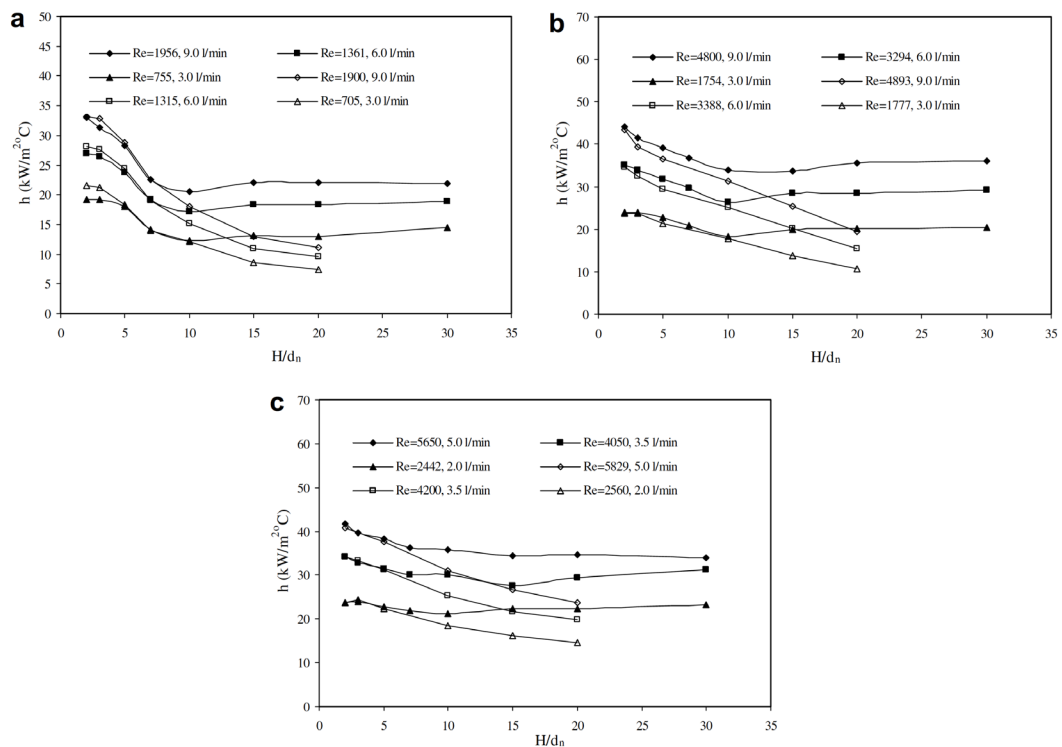
Fig 7. Effect of jet-to-target spacing on the heat transfer for free-surface and confined submerged jets: (a) $S/d_n=3$; (b) $S/d_n=5$; and (c) $S/d_n=7$

Fig. 6 shows that there is a noticeable dependence of the surface average heat transfer with jet-to-target spacing. Although the trend is consistent across all jet-to-jet spacings tested, it is most obvious in Fig. 6a for $S/d_n = 3$. Here, the Nusselt number results cluster together at small ($2 \leq H/d_n \leq 3$) as well as large ($10 \leq H/d_n \leq 30$) jet-to-target spacings. The reduction in Nu_L with increasing H/d_n is attributed to a transition from confined-submerged jet flow to free-surface jet flow, as was pointed out by Pan and Webb [13]. Fig. 7 shows the dependence of the heat transfer with increasing jet-to-target spacing. In the figure, the data for both the free-surface case (i.e. liquid level in vessel below the heater surface) and confined-submerged case (i.e. the liquid level above the nozzle plate) are plotted for identical volumetric flow rates. For jet-to-target spacings below approximately 10, the heat transfer coefficient results of the free and submerged jets are the same. This indicates that, for the free-surface arrangement, the volume of liquid being expelled from the channel separating the heater and the jet nozzle is enough to fill the channel making it behave thermally as a confined-submerged jet array. Beyond approximately $H/d_n = 10$, there is a clear separation of the two curves indicating a change in the mechanism of heat transfer. As previously discussed, the heat transfer coefficient of the submerged jets continues to deteriorate with increasing H/d_n. Converse to this, beyond $H/ d_n = 10$, the free jets no longer spread causing deterioration of the impingement velocity due to entrainment.

Since the jets maintain their structure, the heat transfer to the free-surface jets stops decreasing, and in fact begins to improve somewhat with increasing jet-to-target spacing. This increase of the heat transfer with H/d_n is likely due to destabilisation of the liquid jet that causes break-up of the jet before it strikes the surface [1,18]. This was not investigated in this work. Since the parameter range of this investigation is outside that of previous investigations, it seemed prudent to provide an uncomplicated yet suitably accurate correlating equation of the experimental measurements. Once again, since only one fluid was tested, a Prandtl number dependence of the form $Nu_L \propto Pr^{0.4}$ was selected. Choosing the exponential relation of the form used by Pan and Webb [13] and Fabbri and Dhir [1]. a regression analysis renders the following:

$$\frac{Nu}{Pr^{0.4}} = 7.8 Re_{d_n}^{0.49} \exp\left(-0.025 \frac{S}{d_n}\right) \quad \text{(16)}$$

Fig. 8 shows a comparison of the prediction of Eq. (16) with the experimentally determined surface averaged Nusselt number of this investigation. As it is shown, the correlations predict all of the experimental data within ±10%.
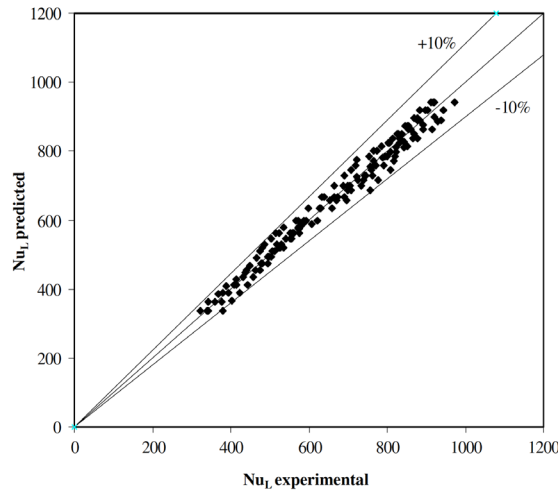

Fig 8. Comparison of the experimental and predicted Nusselt number for free-surface jet arrays for the range $10 \leq H/d_n \leq 30$ and $3 \leq S/d_n \leq 7$.

4.2 Pressure drop and pumping power

Pressure drop measurements across the orifice plate were recorded for each of the tests performed. Generally, there was not a discernable difference between the pressure drop characteristics of the free and submerged jets. Based on the pressure drop data the friction factor was calculated using Eq. (13). The results are plotted in Fig. 9 as a function of Reynolds number for all of the tests performed in this study. The results agree well with the correlation provided by Fabbri and Dhir [1] (Eq. (6)), even though the laser drilling technique used in [1] resulted in inlet and exit holes of unequal size that were not exactly circular and the jets were an order of magnitude smaller than the ones used here. Utilising the same functional form of the relationship a regression analysis of the present data gives,

$$f = 0.51 + \frac{229.9}{Re_{d_n}} \quad \text{(17)}$$

The correlation is able to predict the data to within 25%, as illustrated in the figure. The main result here is that since Eqs. (6) and (17) are so similar, it is proposed that the either expression can be used to predict the pressure drop for microjet to miniature jet arrays with straight through holes within the extended range of $69~\mu m \leq d_n \leq 1.0$ mm.

The correlations developed in this work afford the opportunity to more closely examine the relationship between the heat transfer and the pressure drop for both the submerged-confined and the free-surface jet configurations. The pumping power required to form the jets is related to the pressure drop across the orifice plate, ΔP, and the volumetric flow rate, $\dot{V}$, such that,

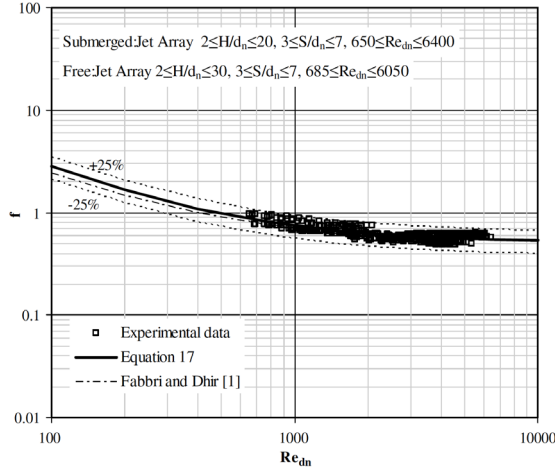$$Q_{pumping} = \dot{V}\Delta P \quad \text{(18)}$$

Fig 9. Friction factor across nozzle plate.

Rearranging Eqs. (11) and (13) for $\dot{V}$ and ΔP respectively, and substituting Eq. (17), the pumping power can be related to the jet Reynolds number,

$$Q_{pumping} = \left[\frac{\pi}{8}\left(\frac{t}{d_n}\right)\left(\frac{\mu^3}{d_n\rho_f^2}\right)N\right]\left[0.51 + \frac{229.9}{Re_{d_n}}\right]Re_{d_n}^2 \qquad (19)$$

Since the magnitude of the pumping power required to achieve a target heat transfer coefficient is of particular interest with regards to electronic thermal packages, Eqs. (14) and (16) were rearranged to isolate the Reynolds number as a function of the heat transfer coefficient for the limiting case of the fully submerged and the entirely free jet configurations;

$$Re_{d_n} = \left(\frac{\bar{h}L_c}{23.39k_f(S/d_n)^{-0.442}(H/d_n)^{-0.0072}Pr^{0.4}}\right)^{2.17} \quad \begin{matrix}\text{Submerged Jet Array}\\ 2 \leq H/d_n \leq 3\end{matrix} \qquad (20)$$

$$Re_{d_n} = \left(\frac{\bar{h}L_c}{7.8k_f\exp\{-0.025(S/d_n)\}Pr^{0.4}}\right)^{2.04} \quad \begin{matrix}\text{Free Jet Array}\\ 10 \leq H/d_n \leq 30\end{matrix} \qquad (21)$$

Eqs. (20) and (21) were substituted into Eq. (19) to generate the curves illustrated in Fig. 10. In the figure, $Q_{pumping}$ is related to the surface averaged heat transfer coefficient, $\bar{h}$, for each flow configuration.

The submerged jet configuration outperforms the free jet configuration for all jet-to-jet spacings tested. The closely spaced (S/d$_n$ = 3) submerged (H/d$_n$ ~ 2) configuration results in the lowest pumping power for a given heat transfer coefficient.
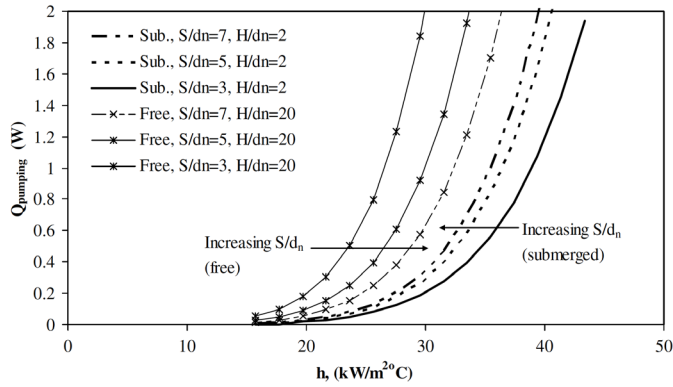
Fig 10. Pumping power required to form jet versus heat transfer coefficient (T_f = 300 K, k_f = 0.631 W/m K, Pr = 5.83).

Conversely, the free-surface jet configuration for S/d_n = 3 results in the highest pumping requirement for a given heat transfer coefficient. Since the curves are somewhat parabolic in shape, the discrepancy in $Q_{pumping}$ between the two flow configurations for a fixed h can be quite extreme. It is also interesting to note that as the jet-to-jet spacing is increased from S/d_n = 3 to S/d_n = 7, the discrepancy between the submerged and free jet configurations diminish. This observation is a result of the fact that for the submerged jets, increasing S/d_n has a detrimental effect with regards to pumping power while increasing S/d_n for the free jets has the opposite effect.

In general, the results indicate that closely spaced submerged liquid jet arrays provide the best performance with regards to the smallest pumping power required to achieve a given heat transfer coefficient. Considering the likelihood that the closely spaced jets will offer the best temperature uniformity as well, this configuration is very suitable for electronics cooling applications. Even still, there is a likely limit to this since if the jet-to-jet spacing is too small, the mechanisms of heat transfer may change as adjacent jets merge with one another resulting in a single well mixed impinging jet structure as opposed to several individual impinging jets

5. Summary

The heat transfer and pressure drop characteristics of liquid jet arrays impinging on a heated surface were investigated for both confined-submerged and free-surface flow configurations. For the submerged jets it was found that the heat transfer is insensitive to changes in the jet-to-target spacing when the nozzle is in close proximity ($2 \leq H/d_n \leq 3$) to the heated surface. For the larger separation distances studied here ($5 \leq H/d_n \leq 20$) the heat transfer deteriorated monotonically with increasing jet-to-target spacing. For a fixed Re_{d_n}, increasing the spacing between jets also had a detrimental effect on the heat transfer. A stronger dependence on jet-to-jet spacing was observed for small jet-to-target spacings as compared with larger ones. The free jet configuration was found to behave thermally as a submerged jet within the range of $2 \leq H/d_n \leq 10$. Beyond this, a transition to entirely free-jet flow occurs and the heat transfer coefficient shows marginal improvement with increasing jet-to-target spacing. Consistent with previous investigation, the measurements here indicate that increasing the jet-to-jet spacing, S/d_n, causes a reduction in the heat transfer for a given Reynolds number. As compared to free-jet flows, the submerged jet configuration at small jet-to-target spacing will provide the required heat transfer coefficient with the smallest pumping power requirement. For the submerged jets, increasing S/d_n causes a decrease in the heat transfer coefficient for a fixed pumping power. Conversely, increasing S/d_n for the free jets at a fixed pumping power causes the heat transfer to increase.

Acknowledgements

References

[1] M. Fabbri, V.K. Dhir, Optimized heat transfer for high power electronics cooling using arrays of microjets, Journal of Heat Transfer 127 (2005) 760–769.

[2] R. Gardon, J.C. Akfirat, The role of turbulence in determining the heat-transfer characteristics of impinging jets, International Journal of Heat and Mass Transfer 8 (1965) 1261–1272.

[3] H. Martin, Heat and mass transfer between impinging gas jets and solid surfaces, in: J.P. Harnett, T.F. Irvine Jr (Eds.), Advances in Heat Transfer, vol. 13, Academic Press, New York, 1977, pp. 1–60.

[4] R.J. Goldstein, K.A. Sobilik, W.S. Seol, Effect of entrainment on the heat transfer to a heated circular jet impinging on a flat surface, Journal of Heat Transfer 112 (1990) 608–611.

[5] J. Stevens, B.W. Webb, Measurements of the free surface flow structure under an impinging, free liquid jet, Journal of Heat Transfer 114 (1992) 79–84.

[6] S.V. Garimella, R.A. Rice, Confined and submerged liquid jet impingement heat transfer, Journal of Heat Transfer 117 (1995) 871–877.

[7] B.W. Webb, C.F. Ma, Single- phase liquid jet impingement heat transfer, in: J.P. Harnett, T.F. Irvine Jr (Eds.), Advances in Heat Transfer, vol. 26, Academic Press, New York, 1995, pp. 105–208.

[8] C.Y. Li, S.V. Garimella, Prandtl-number effects and generalized correlations for confined and submerged jet impingement, Interna- tional Journal of Heat and Mass Transfer 44 (2001) 3471–3480.

[9] N. Gao, D. Ewing, Investigation of the effect of confinement on the heat transfer to round impinging jets exiting a long pipe, International Journal of Heat and Fluid Flow 27 (2006) 33–41.

[10] N. Yonehara, I. Ito, Cooling characteristics of impinging multiple water jets on a horizontal plane, Technology Report Kyushu University 24 (1982) 267–281.

[11] A.M. Kiper, Impinging water jet cooling of VLSI circuits, International Communications in Heat and Mass Transfer 11 (1984) 517– 526.

[12] L.M. Jiji, Z. Dagan, Experimental investigation of single-phase multijet impingement cooling of an array of microelectronic heat sources, in: W. Aung (Ed.), Cooling Technology for Electronic Equipment, Hemisphere Publishing Corporation, Washington, DC, 1988, pp. 333–351.

[13] Y. Pan, B.W. Webb, Heat transfer characteristics of arrays of free-surface liquid jets, Journal of Heat Transfer 117 (1995) 878–883.

[14] D.J. Womac, F.P. Incopera, S. Ramadhyani, Correlating equations for impingement cooling of small heat sources with multiple circular liquid jets, Journal of Heat Transfer 116 (1994) 482–486.

[15] D.J. Womac, F.P. Incopera, S. Ramadhyani, Correlating equations for impingement cooling of small heat sources with single circular liquid jets, Journal of Heat Transfer 115 (1993) 106–115.

[16] S.V. Garimella, B. Nenayedykh, Influence of nozzle geometry on heat transfer in submerged and confined liquid jet impingement, Cooling and Thermal design of Electronic Systems, ASME HTD–319/EEp (1995) 49–57.

[17] P. Brevet, C. Dejeu, E. Dorignac, M. Jolly, J.J. Vulierme, Heat transfer to a row of impinging jets in consideration of optimization, International Journal of Heat and Mass Transfer 45 (2002) 4191– 4200.

[18] S.C. Yao, C.F. Wu, C.C. Hsieh, Microelectromechanical system-based evaporative thermal management of high heat flux electronics, Journal of Heat Transfer 127 (2005) 66–75.

[19] S. Petrovic, T. Robinson, R.L. Judd, Marangoni heat transfer in subcooled nucleate pool boiling, International Journal of Heat and Mass Transfer 47 (2004) 5115–5128.

CONTACT US:

Nexalus Ltd,
Unit 13, South Bank,
Crosse's Green,
Cork, Ireland,
T12 XT71

Nexalus Labs,
Water St,
Loughanalla,
Castlepollard,
Co. Westmeath, Ireland,
N91 EP90

Nexalus Research,
Trinity Research & Innovation,
O'Reilly Institute, Trinity College,
Dublin 2, Ireland,

info@nexalus.com
www.nexalus.com

Registered in Ireland No. 628880,
VAT No. IE3573607SH

WITH ENDORSEMENTS AND SUPPORT FROM:

ENTERPRISE IRELAND
where innovation means business

Science Foundation Ireland
sfi For what's next

Trinity College Dublin
Coláiste na Tríonóide, Baile Átha Cliath
The University of Dublin

CONNECT

IRISH RESEARCH COUNCIL
An Chomhairle um Thaighde in Éirinn

QUALITY CERTIFICATIONS:

IATF 16949 / Automotive Standard
ISO 13485 / Medical Device Standard
ISO 50001 / Energy Management Standard
ISO 45001 / Occupational Heath & Safety Standard
ISO 14001 / Environmental Standard

NEXALUS
COOLING THE CLOUD